

Generation of Bimodal Solitons in a Sapphire Whispering Gallery Mode Maser at Millikelvin Temperatures

Catriona A. Thomson,¹ Michael E. Tobar,¹ and Maxim Goryachev^{1,*}

¹*ARC Centre of Excellence for Engineered Quantum Systems and ARC Centre of Excellence for Dark Matter Particle Physics,
Department of Physics, University of Western Australia,
35 Stirling Highway, Crawley WA 6009, Australia
(Dated: May 23, 2022)*

We present experimental observations of bimodal solitons in a solid state three-level maser cooled to millikelvin temperatures. The maser is built on a highly dilute Fe^{3+} spin ensemble hosted by a high purity Al_2O_3 crystal constituting a high quality factor whispering-gallery-mode resonator. The maser is pumped through one of these modes at around 31 GHz generating two signals around 12.04 GHz from two distinct modes. The system demonstrates three regimes, namely, a highly coherent continuous wave regime, a periodic soliton regime and an incoherent soliton regime. These results open new avenues for studying nonlinear wave phenomena using microwave systems as well as new applications of solitons in this part of the electromagnetic spectrum.

Optical frequency combs have become key in myriad applications from metrology and precision spectroscopy to tests of beyond the standard model physics, with their remarkable ability to compare clocks within 10^{-19} Hz [1, 2]. Initially produced via mode-locked lasers [3–5], which revolutionized the field of frequency metrology [6, 7], a particularly active area of current research is in developing alternative production mechanisms for such combs, in engineering systems balanced between nonlinear gain and dissipation.

A frequency comb may occur in conjunction with coherent solitons within a resonator, that is, ultrashort phase-locked pulses circulating the cavity in the time domain. Such pulses may be infinitely supported within the resonator, given a continuous-wave pump source and a resonant medium which displays a balance between dispersion and non-linear gain [8]. To this end, the nonlinear Kerr effect has been much exploited as the dissipative structure in various material systems [8–10] such as silica optical fibres [11], and high-Q crystalline and silicon nitride-based micro-resonators [8, 12].

Despite such plethora of systems demonstrating combs and solitons [13], they are quite unique to the optical frequency domain. This Letter reports the first, to the best of authors' knowledge, observation of a microwave soliton frequency comb in a maser system. The reported phenomena was produced via the natural iron paramagnetic impurities (order of parts per billion) within the most pure HEMEX grade synthetic sapphire crystal, when cooled to millikelvin temperatures and with zero applied magnetic field [14]. The paramagnetic impurities have been shown to offer non-linear gain in form of a χ^3 non-linearity at 4K in temperature, which besides masing [14], has produced four wave mixing [15], frequency conversion [16] and time reversal symmetry breaking [17, 18]. Furthermore, at millikelvin temperature, effects of paramagnetic impurities on the properties of cooled sapphire

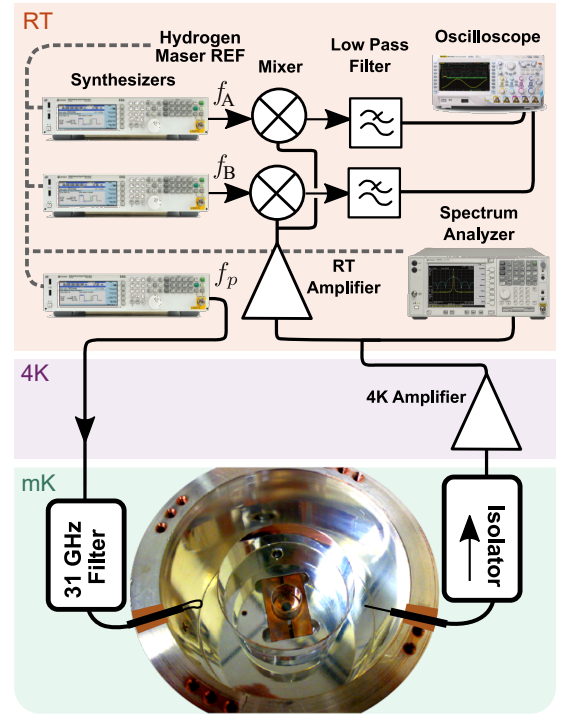


FIG. 1: Experimental setup used to generate maser solitons at mK temperatures. A WGM crystal resonator is pumped from a room temperature signal source (around 31 GHz) through an input filter ensuring minimal excitation of the readout mode. Generated maser signals (around 12 GHz) are collected with a single antenna and fed through a low temperature isolator and a low noise cryogenic amplifier. These signals are analysed via a spectrum analyser and down converted via two mixers to be observed via an oscilloscope.

resonators have been shown to be enhanced when compared with the effects at 4K as the majority of the spins condense to the ground state [18–20]. This work reports the first operation of such a maser at millikelvin temperatures, with the observation of new effects not seen in the 4K system, providing a new avenue for implement-

* maxim.goryachev@uwa.edu.au

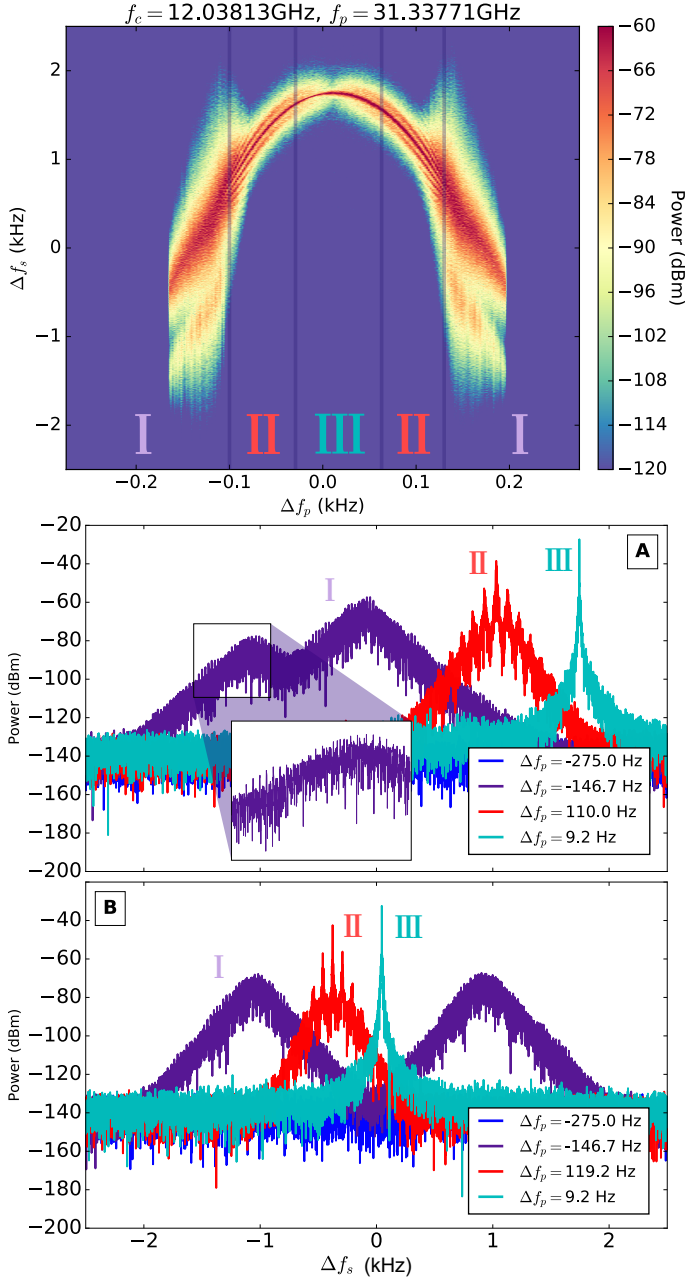


FIG. 2: Top: Spectra of masing on mode A (f_s) for different pump frequencies around 31.3377 GHz (Δf_p). A/B: snapshots of masing on mode A/B at various Δf_p , illustrating the three masing regimes.

ing optical metrological methods in the microwave and radio-frequency domains.

The experimental setup is based on a cylindrical HEMEX grade sapphire (undoped monocrystalline α - Al_2O_3) resonator supporting extremely high quality factor whispering gallery modes (WGMs) in the microwave frequency range. The crystalline lattice of sapphire is host to a number of naturally occurring impurities including Fe^{3+} , Cr^{3+} , and Ti^{3+} with typical concentrations of parts-per-billion in HEMEX-grade crystals [20]. Paramagnetic Fe^{3+} ions in sapphire, each substituting

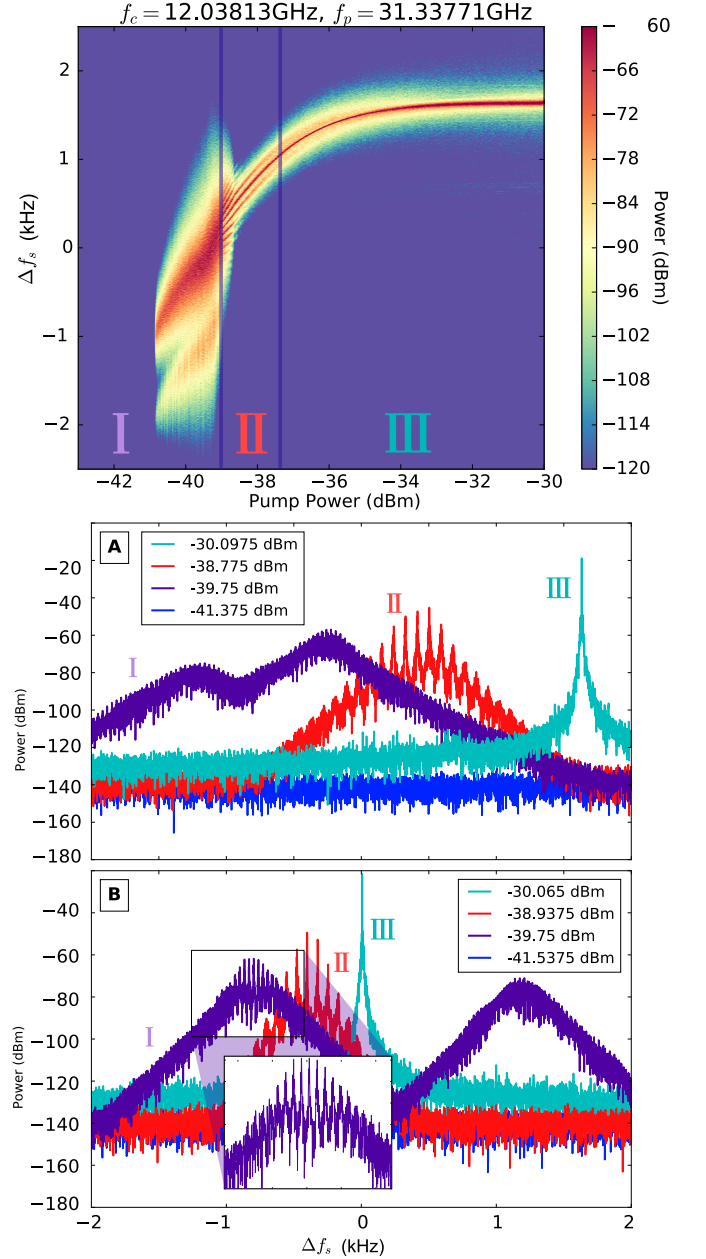


FIG. 3: Top: Spectra of masing on mode A (f_s) for different pump powers at 31.3377 GHz. A/B: snapshots of masing on mode A/B at various pump powers, illustrating the three masing regimes.

an Al^{3+} cation, was proposed [21] and implemented as a gain medium for cryogenic masers, which do not require any external magnetic field [22, 23]. Profitably, at zero applied field, this ion represents a three level system with the spin- $|1/2\rangle$ (ground state), $|3/2\rangle$ (intermediate state), and $|5/2\rangle$ (higher excited) states. These three levels are ideally suited to be used as a Λ -scheme: pumping the $|1/2\rangle \rightarrow |5/2\rangle$ transition via a high-frequency pump WGM within the ion's electron spin resonance (ESR) linewidth, inducing a fast non-radiative transition to the intermediate level with a short life time followed by a ra-

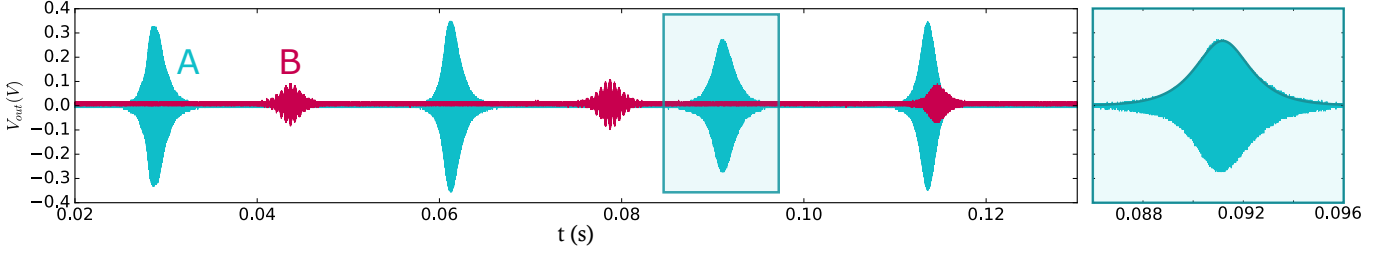


FIG. 4: Times-series output of readout mode A (blue) and B (pink) of the crystal, in regime I, which is being pumped at 31.337707136 GHz, after being mixed down to baseband, representing modulation of the carrier mode. The soliton pulse train is the time-series equivalent of the frequency comb. The fitted *sech* envelope of one pulse is highlighted right. See Supplemental Material for further investigation of the soliton trains.

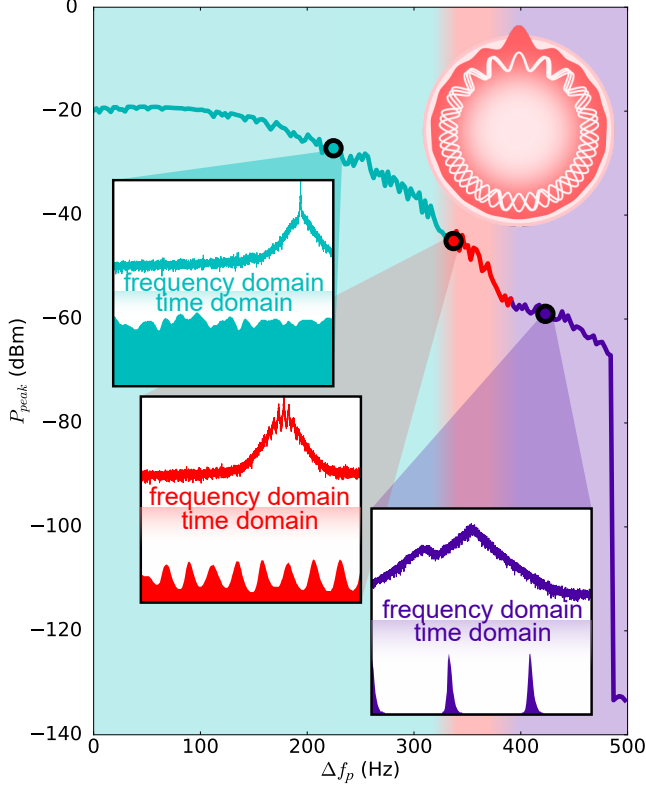


FIG. 5: Maser peak emission (P_{peak}) for various pump frequencies about 31.3377 GHz (Δf_p) for readout mode A, with $P_{pump} = 0$ dBm. Three points are highlighted, one for each regime. The inset panels show maser spectra and associated soliton outputs in the various regimes; (III) single spectral line regime (blue), (II) the few peak regime (red), and (I) the low coherence bimodal regime (purple). Discrete jumps between the regimes can be observed on the spectrum of peak maser output. Top-right inset illustrates the relationship between the comb frequencies, and the intracavity soliton whose existence implies synchronised phases between the comb frequencies.

diative maser transition $|3/2\rangle \rightarrow |1/2\rangle$, stimulating photon emission at the ESR frequencies around ~ 12.04 GHz, which happens to encompass the linewidth of two signal WGMs in the crystal (see Fig 1). These signal WGMs have sufficient quality factors to self-sustain resonance for sufficient pump power.

The sapphire WGM crystal was housed in a silver-

plated copper cavity and interrogated by two microwave probes inserted through the cavity walls. The output probe is an antenna oriented to couple to two modes in the region of 12.04 GHz (specifically, we investigate the responses of readout mode A at 12.03812 GHz and readout mode B at 12.02979 GHz). The input probe is an orthogonally oriented loop which, ideally, strongly couples to the azimuthal magnetic component of one of the (dominantly transverse-magnetic) modes in the vicinity of the 31.9 GHz transition and does not load quality factors of the signal modes, which are quasi-transverse-electric modes.

The cavity is attached to the millikelvin stage of a dilution refrigerator. The pump signal is generated by a microwave synthesizer locked to a hydrogen maser and delivered to the cavity via a series of copper and phosphor-bronze cables. The signal is cleaned by a narrow band-pass filter tuned to near 31.5 GHz and directly bolted to the cavity. The total attenuation of the cables and the filter from the output of the synthesizer to the input of the cavity is 31 dB at the pump frequency. The output signals from the crystal pass through a millikelvin isolator and a 4 K low noise amplifier. At room temperature the target signal is split between a spectrum analyzer, used to collect frequency data around the target mode, and two downconversion channels, used to mix down the signal for collection of time-series data. To achieve downconversion, two synthesizers generate frequencies of f_A and f_B to bring the signal carriers to the kHz level whereby they are individually digitized with a two-channel high-speed real-time oscilloscope. A schematic of the experimental setup used to observe maser solitons is shown in Fig. 1.

Masing was observed on two signal modes ($f_A = 12.03813$ GHz and $f_B = 12.02979$ GHz) for a range of pump frequencies, Δf_p , swept around the pump mode, $f_p = 31.33771$ GHz. Full spectra of the masing signal from f_A is given in Fig 2, along with snapshots from both f_A and f_B . At millikelvin temperatures (within a dilution fridge cooled to ~ 16 mK, but transiently heated to ~ 20 -50 mK), a fine frequency comb was obtained, the first maser comb observed to the knowledge of the authors (Figs. 2 and 3, inset). Data at 4 K were also obtained, but results are deferred to the Supplemental Material.

Fig. 2 and 3 demonstrate three distinct generation

regimes: (III) the continuous wave regime at the centre (near zero Δf_p) with a narrow masing peak, (II) the few peak regime for larger detuning, corresponding to high density soliton emission, followed by (I), a low coherence broad spectrum regime just surpassing the masing threshold on both sides of the masing regime, with few solitons. The latter regime demonstrates a second broad feature that can be attributed to the doublet phenomenon in WGM systems where the solution has two degenerate components. Various symmetry breaking features in the sapphire resonator lift this degeneracy and our readout mode thus exists as a double peaked structure. It is worth noting that for the highly coherent regime with $\Delta f_p \sim 0$, one peak supercedes the other within the doublet. The dependance of the masing regime upon explicitly pump power, at a fixed pump frequency, was also clearly observed (see Fig. 3), displaying analogous regimes to the detuned frequency experiment, due to the lineshape of the pump mode.

Examining the time-series data, this masing can be observed to be expelled in discrete millisecond-scale solitons, the time-domain phenomenon associated with the observed frequency comb. The emission of discernible pulses can be observed up to a saturation point, corresponding to coherent single-frequency maser emission (cyan in Fig. 3). The relationship between comb shape and soliton emission period is illustrated in Fig. 5, which maps out the three regimes, dependant upon pump frequency. These observations provide a window into

the spontaneous self-organization behaviours within this nonlinear many-body spin system, worthy of further study. The system may be described by the Lugiato-Lefever equation (a damped, driven, non-linear wave equation) for which temporal solitons on top of a continuous wave pump are a solution and which likewise describes the dynamics of Kerr frequency combs [24]. The dispersion profile of the solitons and the period of emission can be controlled via our two variable parameters, pump power and pump frequency. These temporal results are more thoroughly presented in the Supplemental Material.

The production of this maser-based frequency comb, and associated soliton pulse train, in a simple sapphire system has great potential for further investigation, both theoretically, into the behaviour of the dissipative masing system, and into the potential applications of this comb, for example in precision spectroscopy [6], tunable narrowband microwave signal generation [25] or reconfigurable RF filtering [26]. Detailed characterization of the frequency comb and soliton evolution will be undertaken in the future.

Acknowledgements

This research was supported by the ARC Centre of Excellence for Engineered Quantum Systems (EQUS, CE170100009) and the ARC Centre of Excellence for Dark Matter Particle Physics (CDM, CE200100008).

-
- [1] Th. Udem, R. Holzwarth, and T. W. Hänsch. Optical frequency metrology. *Nature*, 416(6877):233–237, mar 2002.
 - [2] Scott A Diddams, Kerry Vahala, and Thomas Udem. Optical frequency combs: Coherently uniting the electromagnetic spectrum. *Science*, 369(6501), 2020.
 - [3] M. Kourogi, K. Nakagawa, and M. Ohtsu. Wide-span optical frequency comb generator for accurate optical frequency difference measurement. *IEEE Journal of Quantum Electronics*, 29(10):2693–2701, 1993.
 - [4] Th. Udem, J. Reichert, R. Holzwarth, and T. W. Hänsch. Accurate measurement of large optical frequency differences with a mode-locked laser. *Optics Letters*, 24(13):881, jul 1999.
 - [5] J. Reichert, R. Holzwarth, Th. Udem, and T.W. Hänsch. Measuring the frequency of light with mode-locked lasers. *Optics Communications*, 172(1-6):59–68, dec 1999.
 - [6] Scott A. Diddams, Leo Hollberg, and Vela Mbele. Molecular fingerprinting with the resolved modes of a femtosecond laser frequency comb. *Nature*, 445(7128):627–630, February 2007.
 - [7] S. Witte. Deep-ultraviolet quantum interference metrology with ultrashort laser pulses. *Science*, 307(5708):400–403, jan 2005.
 - [8] Xu Yi, Qi-Fan Yang, Ki Youl Yang, Myoung-Gyun Suh, and Kerry Vahala. Soliton frequency comb at microwave rates in a high-q silica microresonator. *Optica*, 2(12):1078, dec 2015.
 - [9] A. Barthelemy, S. Maneuf, and C. Froehly. Propagation soliton et auto-confinement de faisceaux laser par non linearité optique de kerr. *Optics Communications*, 55(3):201–206, sep 1985.
 - [10] Cyril Cambournac, Hervé Maillotte, Eric Lantz, John M. Dudley, and Mathieu Chauvet. Spatiotemporal behavior of periodic arrays of spatial solitons in a planar waveguide with relaxing kerr nonlinearity. *Journal of the Optical Society of America B*, 19(3):574, mar 2002.
 - [11] François Leo, Stéphane Coen, Pascal Kockaert, Simon-Pierre Gorza, Philippe Emplit, and Marc Haelterman. Temporal cavity solitons in one-dimensional kerr media as bits in an all-optical buffer. *Nature Photonics*, 4(7):471–476, may 2010.
 - [12] T. Herr, V. Brasch, J. D. Jost, C. Y. Wang, N. M. Kondratiev, M. L. Gorodetsky, and T. J. Kippenberg. Temporal solitons in optical microresonators. *Nature Photonics*, 8(2):145–152, dec 2013.
 - [13] Tara Fortier and Esther Baumann. 20 years of developments in optical frequency comb technology and applications. *Communications Physics*, 2(1):153, 2019.
 - [14] P.-Y. Bourgeois, N. Bazin, Y. Kersalé, V. Giordano, M. E. Tobar, and M. Oxborrow. Maser oscillation in a whispering-gallery-mode microwave resonator. *Applied Physics Letters*, 87(22):224104, 2005.
 - [15] Daniel L. Creedon, Karim Benmessaï, Warwick P. Bowen, and Michael E. Tobar. Four-wave mixing from Fe^{3+} spins in sapphire. *Phys. Rev. Lett.*, 108:093902, Feb

- 2012.
- [16] Daniel L. Creedon, Karim Benmessai, and Michael E. Tobar. Frequency conversion in a high q -factor sapphire whispering gallery mode resonator due to paramagnetic nonlinearity. *Phys. Rev. Lett.*, 109:143902, Oct 2012.
 - [17] K. Benmessai, M.E. Tobar, N. Bazin, P-Y. Bourgeois, Y. Kersalé, and V. Giordano. Creating traveling waves from standing waves from the gyrotropic paramagnetic properties of Fe^{3+} ions in a high- q whispering gallery mode sapphire resonator. *Physics Review B*, 79(17):174432, 2009.
 - [18] Maxim Goryachev, Warrick G. Farr, Daniel L. Creedon, and Michael E. Tobar. Spin-photon interaction in a cavity with time-reversal symmetry breaking. *Phys. Rev. B*, 89(22):224407–, June 2014.
 - [19] Daniel L. Creedon, Yarema Reshitnyk, Warrick Farr, John M. Martinis, Timothy L. Duty, and Michael E. Tobar. High q -factor sapphire whispering gallery mode microwave resonator at single photon energies and millikelvin temperatures. *Appl. Phys. Lett.*, 98(22):–, 2011.
 - [20] Warrick G. Farr, Daniel L. Creedon, Maxim Goryachev, Karim Benmessai, and Michael E. Tobar. Ultrasensitive microwave spectroscopy of paramagnetic impurities in sapphire crystals at millikelvin temperatures. *Phys. Rev. B*, 88:224426, December 2013.
 - [21] L.S. Kornienko and A.M. Prokhorov. Electronic paramagnetic resonance of the Fe^{3+} ion in corundum. *J. Exp. Theor. Phys.*, 40:1594–1601, 1961.
 - [22] Karim Benmessai, Daniel Lloyd Creedon, Michael Edmund Tobar, Pierre-Yves Bourgeois, Yann Kersalé, and Vincent Giordano. Measurement of the fundamental thermal noise limit in a cryogenic sapphire frequency standard using bimodal maser oscillations. *Phys. Rev. Lett.*, 100(23):233901–, June 2008.
 - [23] D. L. Creedon, K. Benmessai, M. E. Tobar, J. G. Hartnett, P. Bourgeois, Y. Kersale, J. Le Floch, and V. Giordano. High power solid-state sapphire whispering gallery mode maser. In *2009 IEEE International Frequency Control Symposium Joint with the 22nd European Frequency and Time forum*, pages 282–285, 2009.
 - [24] L. A. Lugiato, F. Prati, M. L. Gorodetsky, and T. J. Kippenberg. From the lugiato-lefever equation to microresonator-based soliton kerr frequency combs. *Philosophical Transactions of the Royal Society A: Mathematical, Physical and Engineering Sciences*, 376(2135):20180113, November 2018.
 - [25] Nathan R. Newbury. Searching for applications with a fine-tooth comb. *Nat. Photonics*, 5(4):186–188, March 2011.
 - [26] Anatoliy A. Savchenkov, Andrey B. Matsko, Vladimir S. Ilchenko, Iouri Solomatine, David Seidel, and Lute Maleki. Tunable optical frequency comb with a crystalline whispering gallery mode resonator. *Physical Review Letters*, 101(9), aug 2008.

Supplemental Material for:

Generation of Bimodal Solitons in a Sapphire Whispering Gallery Mode Maser at Millikelvin Temperatures

In this supplemental material, we present further results from the experiment described in the main body of the Letter. In particular, masing on the second pump mode, full plots of masing produced by the readout mode B, masing at 4 K and time-series soliton data at mK is presented.

Target Whispering Gallery Modes

Pump Mode	Frequency (GHz)	Readout Mode	Frequency (GHz)
Pump Mode 1	31.33771	Readout Mode A	12.03812
Pump Mode 2	31.33974	Readout Mode B	12.02979

I. Results at 4 K

Fig. 6 presents the power-dependence of masing, for readout modes A and B. Unlike the masing results at mK, shown in the main paper, there is no two peak structure present, and although there are modulation sidebands, a fine frequency comb is not produced as in the mK case. Fig 7 presents the response of masing on modes A and B when the pump frequency is swept. As in the mK case, the doublet structure of the pump mode is evident.

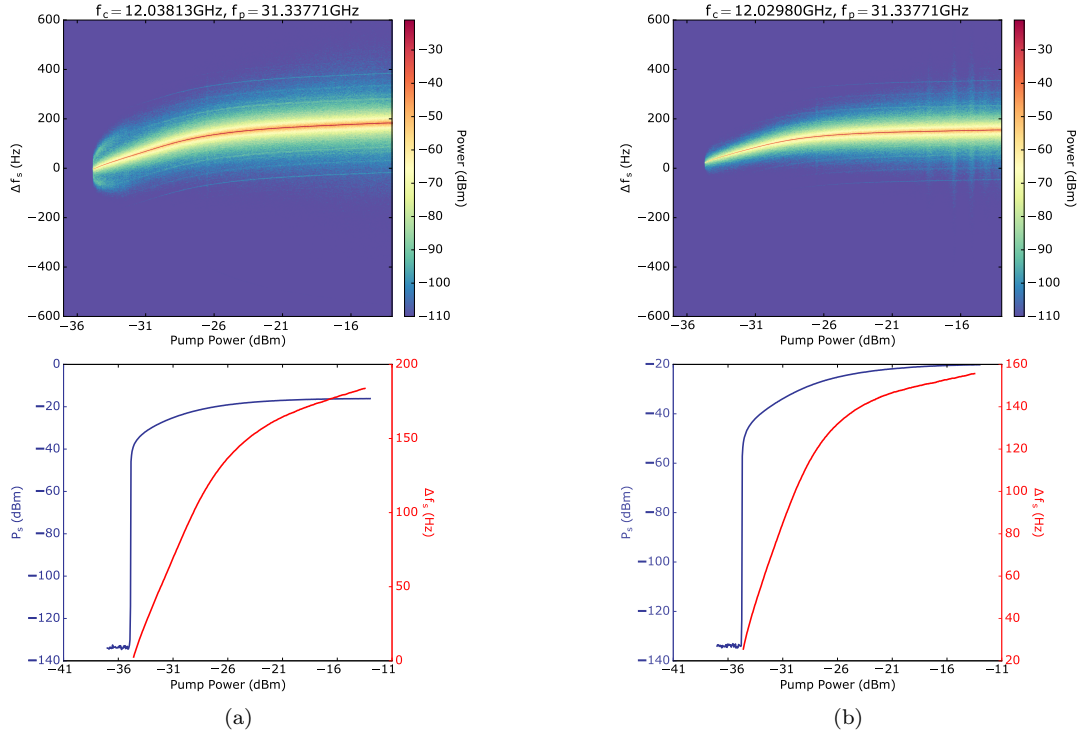


FIG. 6: Pumping on the first pump mode at an array of pump powers for readout modes A (a) and B (b). Measurements taken at 4 K. Power at signal output is gauged by the color bar and the masing peak can be tracked relative to the centre of the measurement spectrum (Δf_s). The bottom plots isolate the frequency drift (Δf_s , red) and maximum power (P_s , purple) of the maser peaks, depending on input pump power.

II. Further Results at mK

Fig. 8 and 9 present masing observed at mK, that is, between 16 mK and 50 mK after transient heating, additional to the plots shown in the main paper, over a range of pump frequencies and at different input powers. Fig. 8 presents results when pump mode 1 was pumped and Fig. 9 presents results when pump mode 2 was pumped.

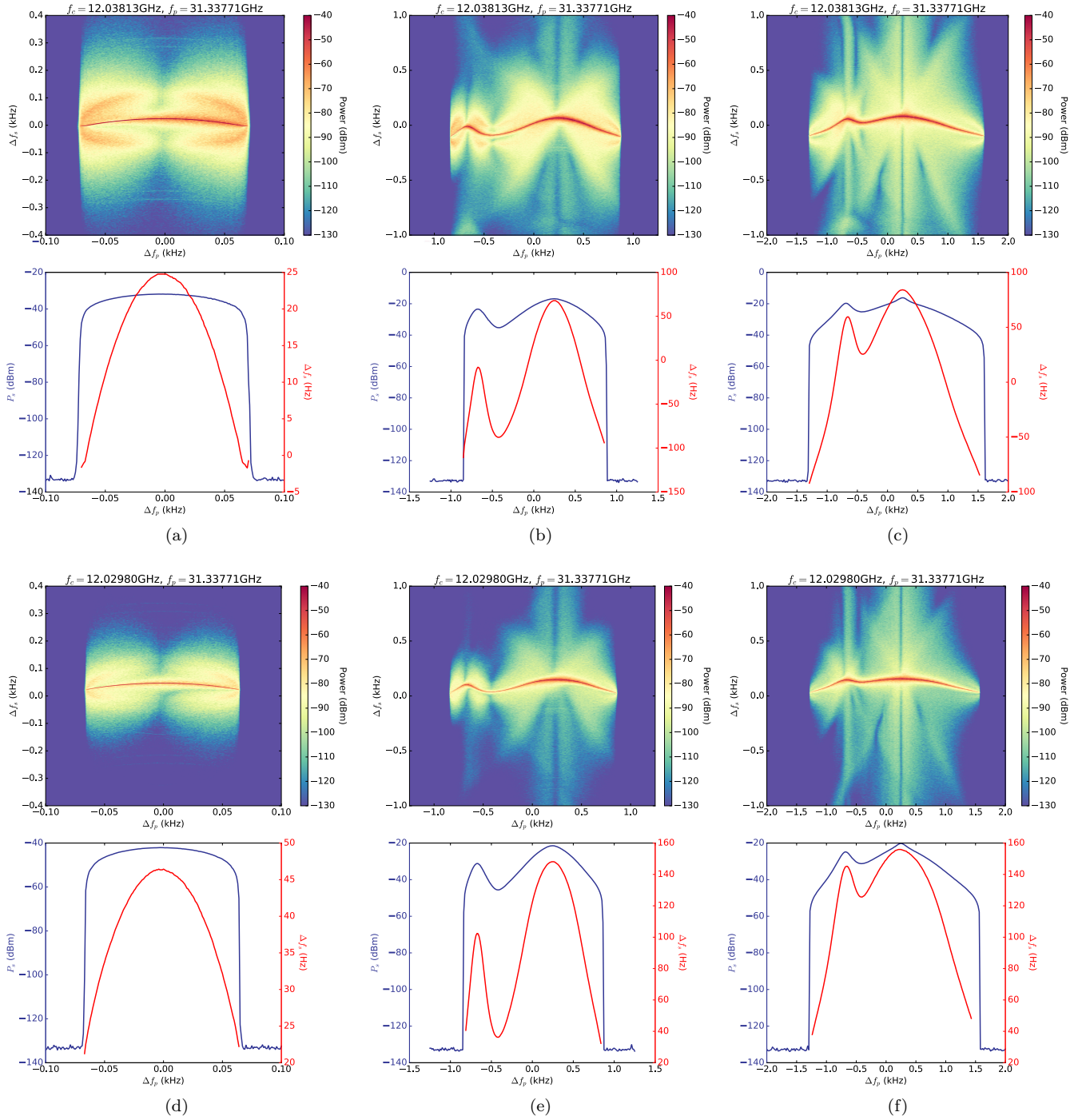


FIG. 7: Pumping on the first pump mode at an array of pump frequencies about f_p for readout modes A (a,b,c) and B (d,e,f) with pump power set to -33 dBm, -20 dBm and -13 dBm respectively. Measurements taken at 4 K. Power at signal output is gauged by the color bar and the masing peak can be tracked relative to the centre of the measurement spectrum (Δf_s). The bottom plots isolate the frequency drift (Δf_s , red) and maximum power (P_s , purple) of the maser peaks, depending on input pump frequency.

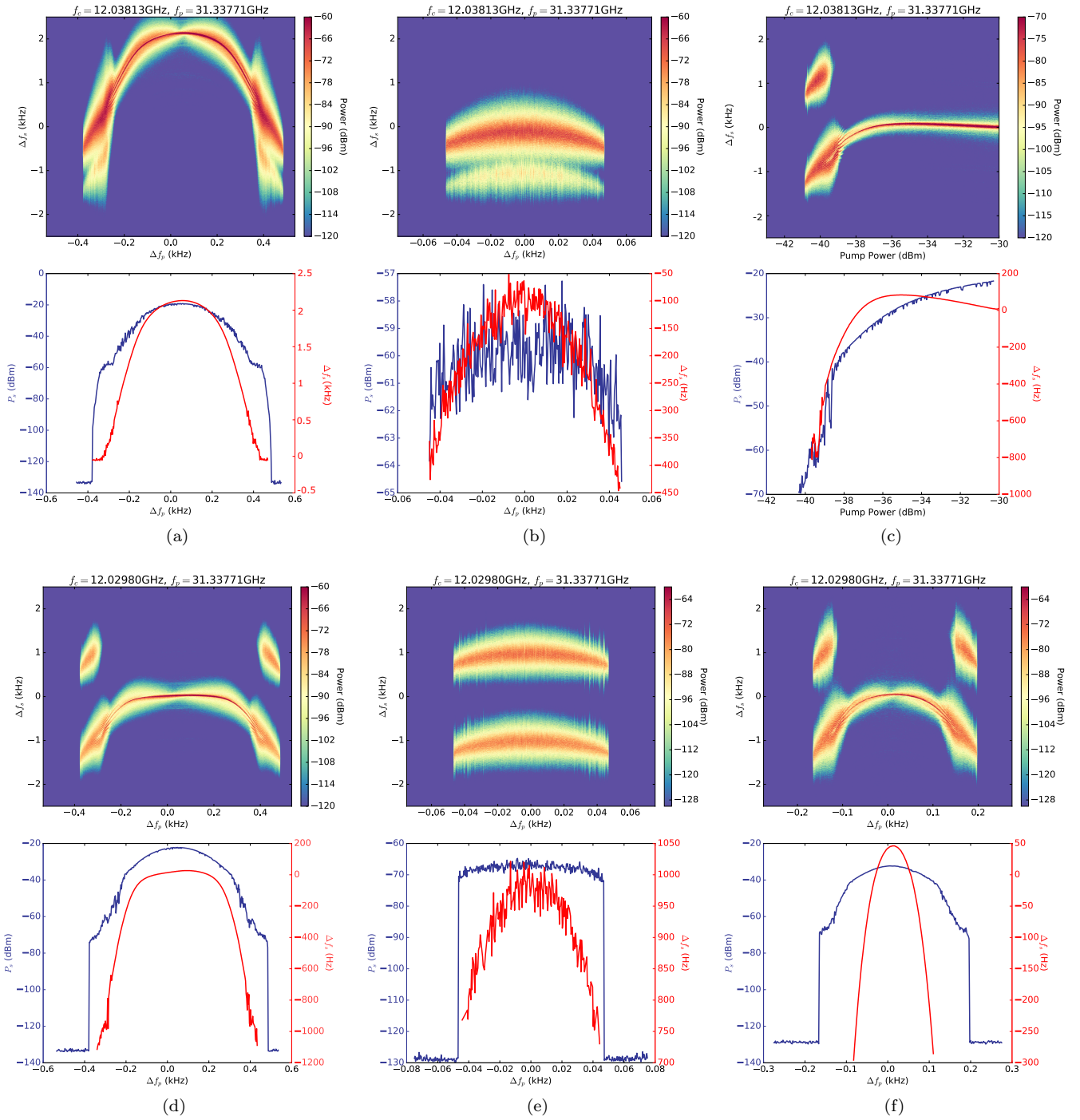


FIG. 8: Pumping on the first pump mode at an array of pump frequencies about f_p for readout modes A (a,b) and B (d,e,f) with pump power set to -31 dBm, -41 dBm and -37 dBm (mode B only) respectively. Measurements taken at mK. Power at signal output is gauged by the color bar and the masing peak can be tracked relative to the centre of the measurement spectrum (Δf_s). The bottom plots isolate the frequency drift (Δf_s , red) and maximum power (P_s , purple) of the maser peaks, depending on input pump frequency. The dependance of readout mode B upon pump power is represented in (c), but neglected for mode A, as this is shown in the main paper.

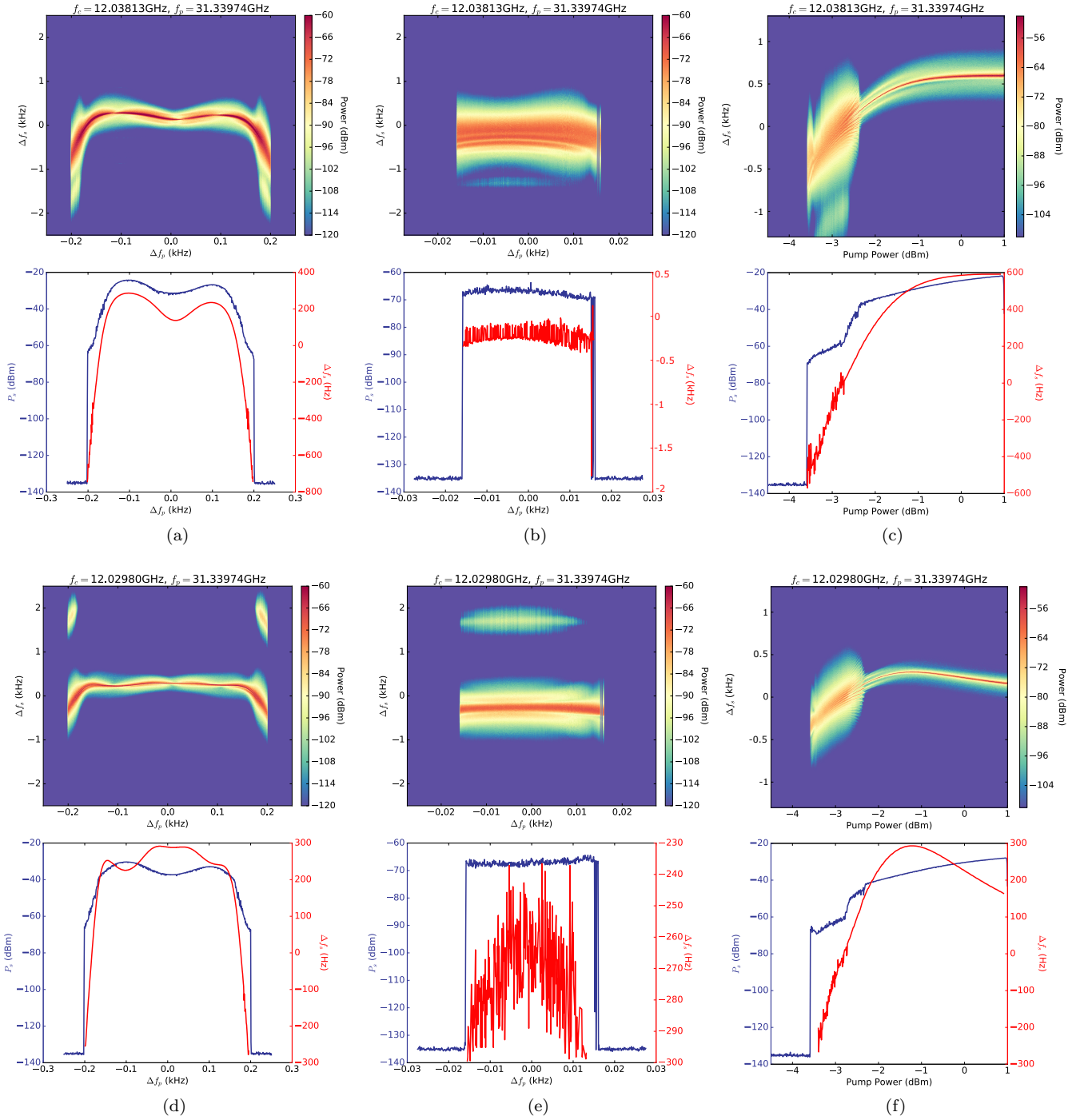


FIG. 9: Pumping on the first pump mode at an array of pump frequencies about f_p for readout modes A (a,b) and B (d,e) with pump power set to -31 dBm and -34.5 dBm respectively. Measurements taken at mK. Power at signal output is gauged by the color bar and the masing peak can be tracked relative to the centre of the measurement spectrum (Δf_s). The bottom plots isolate the frequency drift (Δf_s , red) and maximum power (P_s , purple) of the maser peaks, depending on input pump frequency. The dependence of readout modes A and B upon pump power is also represented ((c) and (f)).

III. Soliton Pulse Trains at mK

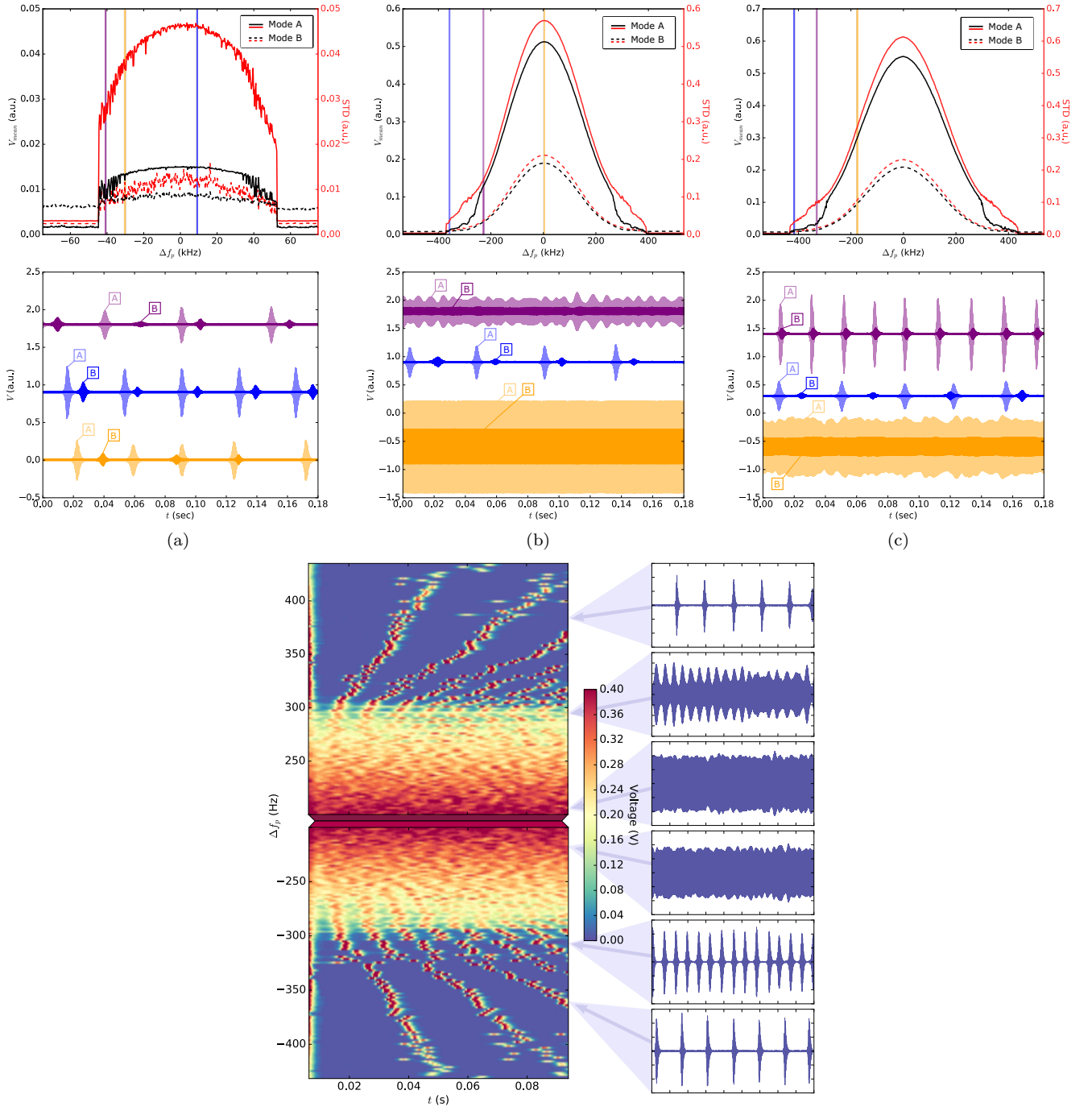


FIG. 10: At input powers of -41 dBm, -36 dBm and -31 dBm ((a),(b), and (c)), the pump frequency was swept around pump mode 1 (Δf_p), and solitons were observed at the mixed down readout mode outputs A and B. The top plots record the standard deviation (red) and mean output voltage (black) of the soliton train (or continuous wave) emanating from the crystal at the signal modes. Depending on the input pump frequency, solitons may be emitted discretely in pulses, or the output may evolve into a continuous wave. The bottom plot (right) presents snapshots of the soliton output produced at -31 dBm input (corresponding to (c)), for various Δf_p . In the color density plot, traces are aligned to the first pulse to illustrate intersoliton-period dependence upon pump frequency.

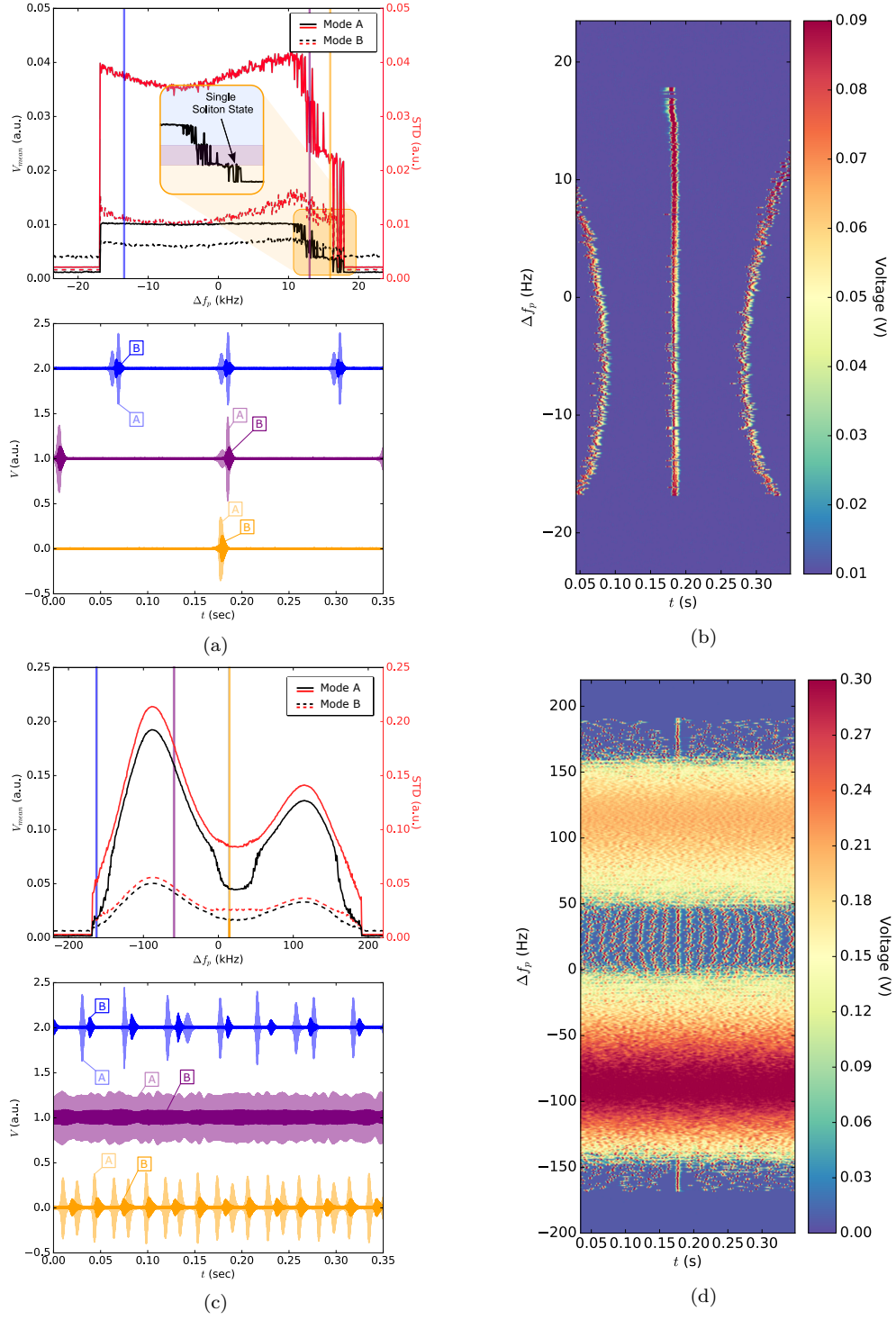


FIG. 11: At input powers of -34.5 dBm ((a) and (b)) and -32 dBm ((c) and (d)), the pump frequency was swept around pump mode 2, and solitons were observed at the mixed down readout mode outputs A and B. The left plots record the standard deviation (red) and mean output voltage (black) of the soliton train (or continuous wave) emanating from the crystal at the signal modes. Plots (b) and (d) present snapshots of the soliton output produced at -34.5 dBm and -32 dBm input, from mode A and B respectively, for various Δf_p . In the latter, we can observe the pump twice breaching the power level at which discrete soliton emission can be sustained, caused by the doublet shape of the pump mode. Highlighted in (a), the mean output voltage shows clear jumps at certain Δf_p steps, which suggests the elimination of one intracavity soliton at each step. The yellow region (corresponding to the yellow time-trace) is therefore representative of the single soliton state.